Experimental Research on Impulse Coupling Characteristics and Plasma Plume Dynamics of a Nanosecond Pulsed Laser Irradiated Aluminum Target

CHENGHAO YU[ID], WEIJING ZHOU[ID], HAO CHANG[ID], AND YIFU CHEN[ID]

State Key Laboratory of Laser Propulsion & Application, Department of Aerospace and Technology, Space Engineering University, Beijing 101416, China

Corresponding authors: Weijing Zhou (viviazhouyy@163.com) and Hao Chang (changhao5976911@163.com)

ABSTRACT The impulse generated by ablating aluminum targets was investigated in this study using the micro-impulse measurement method with a torsion pendulum, and the plasma plume characteristics were researched using fast photography and optical emission spectroscopy. The experiment was carried out with a pulsed laser with a wavelength of 1064 nm and a pulse duration of 8.7 ns. The fluence varied from 5.69 J/cm² to 33.67 J/cm². The impulse coupling coefficients were obtained from the impulse measurements and the images of the plasma plume were recorded with a gate width of 500 ns. The results indicated that the variation of the impulse coupling coefficient was affected by the change of the laser fluence and the decline of the coefficient at high fluence was because of the plasma shielding effect. The intense radiation region located above the target surface in the corresponding plume was evident. Additionally, the differential coupling coefficient was presented and compared with the impulse coupling coefficient. The plasma temperature and the electron number density were estimated with the Boltzmann plot method and the Stark broadening method, respectively, using optical emission spectroscopy. Furthermore, the relative energy coupling efficiency was deduced from the plume front positions to determine the influence of the plume expansion dynamics on the impulse coupling. The obtained results showed that the variation trend of efficiency versus the laser fluence was similar to that of the impulse coupling coefficient.

INDEX TERMS Laser ablation, impulse coupling coefficient, fast photography, plasma shielding effect, energy coupling efficiency.

I. INTRODUCTION

In recent years, there has been an increasing amount of research on the process of laser ablation because of its wide applications in pulsed laser deposition [1], laser hardening [2], laser polished surfaces [3], laser materials processing [4], laser-induced breakdown spectroscopy [5] and pulsed laser ablation propulsion [6]. Among these applications, pulsed laser ablation propulsion (LAP) shows potential solutions for some space fields of growing importance, such as space debris removal [7], laser ablation micro-thrusters for orbit and attitude control of nano-satellites [8], and the despinning of non-cooperative space objectives remotely [9].

The associate editor coordinating the review of this manuscript and approving it for publication was Zhenbao Liu[ID].

These applications in space are mainly due to the recoil impulse generated by a rapidly expanding ablation plume away from a target surface [10]. Hence, the fundamentals of pulsed laser ablation plumes and their effects on a generation impulse have attracted a great deal of attention.

To date, extensive studies have been conducted on impulse characteristics under various conditions, including laser parameters [11], ambient gas pressures [12], laser incident angles [13], and the materials of the targets [14]. To obtain the characteristics of ablation impulses, the typical measurement techniques, including torsion pendulums [15] and perpendicular pendulums [13], were often used. The thrust performance of LAP is commonly evaluated with the impulse coupling coefficient C_m, which is the ratio of the impulse generated by laser ablation to the incident laser energy [15]. The variation

of C_m observed by most studies revealed that its value was greatly influenced by the expansion dynamics of the ablation plumes [16]. Therefore, it is necessary to study the plume expanding dynamics caused by pulsed laser ablation. To date, some common techniques have been adopted to analyze plume dynamics such as fast photography [17], shadowgraphs [18], optical emission spectroscopy [19], and Faraday cups [20]. Additionally, the resulting spatiotemporal shock wave propagation [18], the emission intensity of excited ions or atoms [21], and the electron number density [17] were often investigated in tests. However, there has been little discussion about the impact of plume expansion dynamics on the thrust performance of LAP. In practice, the structure and the time-resolved expansion process of an ablation plume has an important effect on the ablation impulse exerting to a target [16]. Therefore, it is necessary to investigate the influence of plume propagation dynamics on a generated impulse.

For LAP, a high laser fluence is often used and the resulting plasma plume is an important critical phenomenon [11]. The relationship between an impulse and a plasma plume is the key to describing the LAP performance. In this study, the impulse generated by nanosecond pulsed laser ablation on an aluminum target was obtained with a torsion pendulum, and the plasma plume maps at different laser fluences and different time delays were simultaneously visualized with fast photography. The comparisons between the plume structure and the impulse coupling coefficient were carried out to generalize the relationships between the ablation impulse and the plume. To further analyze the influence of ablation plume on impulse coupling characteristics, the plasma temperature and the electron number density were estimated with the Boltzmann plot method and the Stark broadening method, respectively, using optical emission spectroscopy (OES). Furthermore, the relative energy coupling efficiency was deduced from the plasma emission front of the time-resolved plume maps to obtain a better understanding of the effects on the impulse coupling characteristics.

II. EXPERIMENTAL SETUP

The setup of the experiment is shown in Fig. 1. The system, which was laid in a 10^{-2} Pa environment in a vacuum chamber, was established to measure the generated impulse of the laser irradiation and to take photographs of the laser ablation-induced plasma simultaneously. A neodymium: yttrium-aluminum-garnet (Nd: YAG) laser was used as the energy source to ablate an aluminum target (Al 5A06). The pulse duration (full width at half maximum) and the wavelength of the laser were 8.7 ns and 1064 nm, respectively. The radiance profile of the focused laser spot had an approximately Gaussian distribution. For this experiment, by using a 150mm plano-convex lens, the pulsed laser was focused vertically onto the surface of the target. The distance between the focal lens and the target surface was kept constant. In the experiment, the laser pulse energy delivered to the target surface ranged from 55.1 mJ to 603 mJ. Based on the method
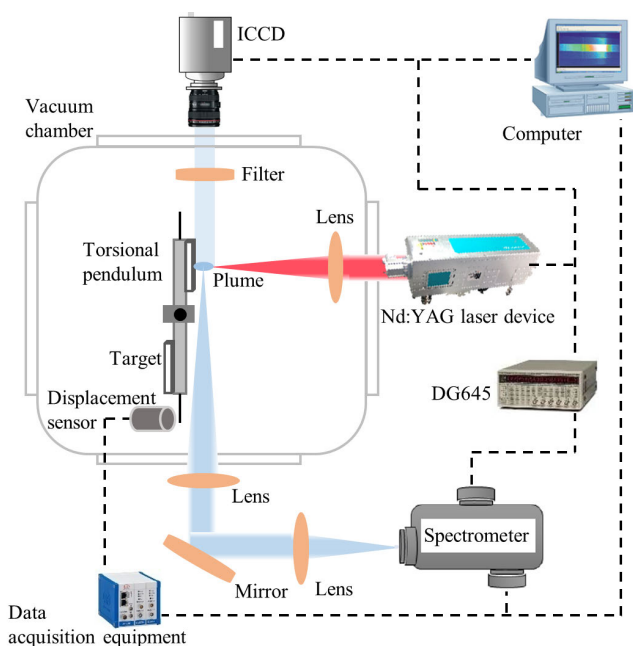
FIGURE 1. Schematic of the experimental setup used for the laser ablation impulse and the plasma plume measurement. The torsion pendulum was used to measure the micro-impulse generated by the pulsed laser ablation. The ICCD camera was used to record the time-resolved images of the fast-moving plasma plume. The spectrometer was used to study the optical emission spectra of the Al plasma plume. The dotted lines show the triggering and data acquisition channels.
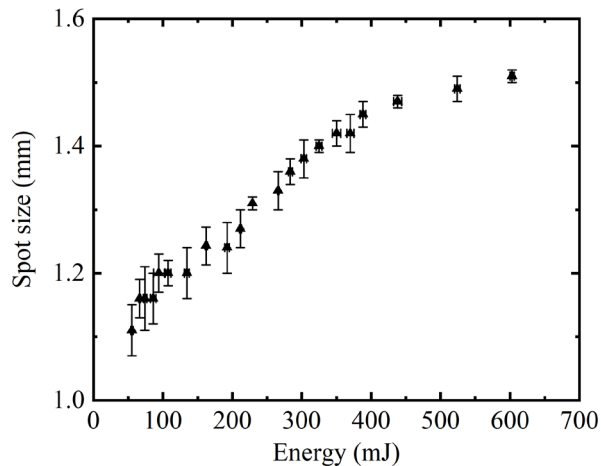
FIGURE 2. The spot size generated by different input laser energies.

proposed by Tsuruta *et al.* [14], the corresponding spot size ranged from 1.11 mm to 1.51 mm as shown in Fig. 2. To ensure the accuracy of the energy measurement, an energy meter (FieldMax, Coherent) was used to measure the pulsed laser energy reaching the aluminum target surface before and after the experiment. In the tests, the energy uncertainty of the pulse-to-pulse laser did not exceed 4%. The ablation mass was weighed with a high-precision electronic balance (XS105DU, Mettler Toledo). A motorized translation stage was installed under the torsion pendulum to change the

ablation position on the target so that a new surface area on the target could be ensured for every laser pulse.
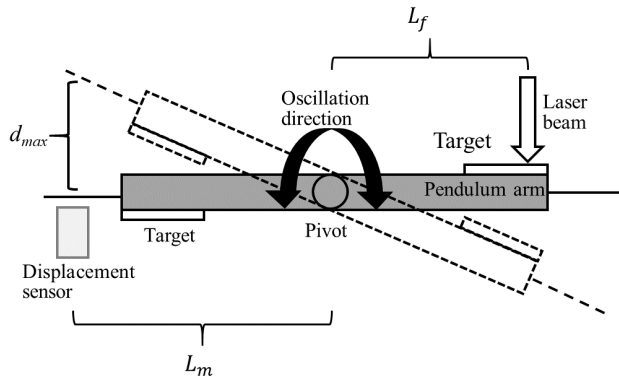

FIGURE 3. Schematic of the setup for the impulse measurement. The diagram shows the arrangement of the target, the pendulum arm, the displacement sensor, and the pivot.

FIGURE 4. An example of the rotational angle of the torsion pendulum.

The torsion pendulum device was employed to measure the micro impulse generated by the laser irradiating the aluminum target. The top view of the pendulum is shown in Fig. 3. When a laser pulse irradiated the target surface, the interaction resulted in the generation of an ablation plume which caused the pendulum arm to oscillate. In the experiment, the deflection angles were measured using a displacement sensor (2 mm range, sensor CSE2, MICRO-EPSILON Company). The detailed principles of micro impulse measurement with a torsion pendulum are described in references [22] and [23]. According to the principle, the impulse calculation form could be expressed as follows:

$$I = \frac{J\omega_n}{L_f L_m} \exp\left(\frac{\zeta}{\sqrt{1-\zeta^2}} \arctan \frac{\sqrt{1-\zeta^2}}{\zeta}\right) d_{\max} \quad (1)$$

where I, J, and ω_n indicate the impulse, the moment of inertia, and the inherent angular frequency, respectively. The symbols L_f, L_m, and ζ denote the arm of force, the measuring arm, and the damping ratio, respectively. $d_{\max}$ is the maximum displacement measured by the displacement sensor after the pulse laser ablation of the aluminum target. A typical rotation angle for the torsional pendulum is shown in Fig. 4. The natural period was 2.07 s, and the max rotation angle was only about 4×10^{-4} rad. The system developed in the test could measure the impulse in the range of 10^{-7} - 10^{-5} N·s.

A high-speed ICCD (TRC311-S-HQB, Intelligent Scientific Systems) was placed perpendicular to the normal direction of the target surface, and it was used to visualize and record the plasma plume structures with different delay times and varied laser fluences. The visible plasma radiation induced by the pulsed laser could be recorded in a wavelength range of 400-800 nm [24]. The spectrally resolved images of the plasma were recorded by a grating spectrograph. Temporal resolution was achieved by using a digital delay pulse generator (DG645, Stanford Research Systems) that triggered the ICCD and the laser for the zero and the delay time.
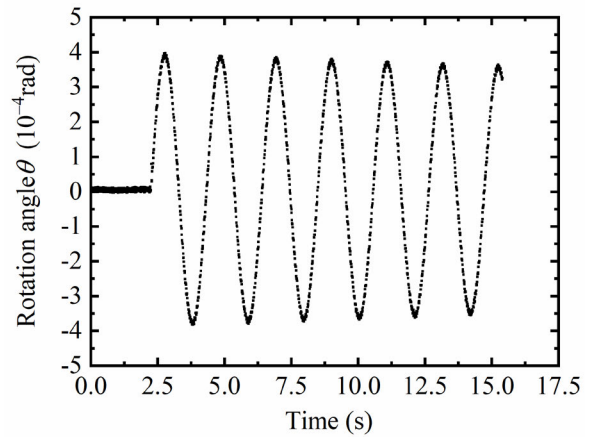
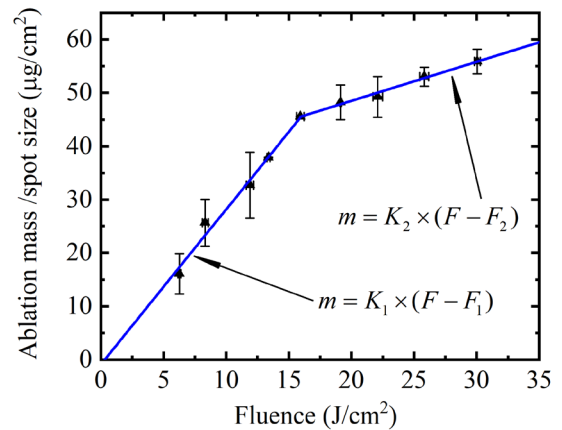The spatial-resolution was achieved by using a combination of lenses in the experiment.

FIGURE 5. Diagram illustrating the variation of the (ablation mass)/(spot size) irradiated by different laser fluences. The two solid lines (blue) represent fitting with a straight line function respectively. Where *m* and *F* represent the (ablation mass)/(spot size) and laser fluence, respectively. $K_1 = 2.906\mu g/J$, $F_1 = 0.3052 J/cm^2$, $K_2 = 0.7308\mu g/J$, and $F_2 = -46.38 J/cm^2$ were obtained by the least squares method.

III. RESULTS AND DISCUSSION

A. ABLATION IMPULSE

The ablation mass had an important influence on the formation of the impulse. The ablation mass per laser pulse was calculated by measuring the accumulating ablation mass through a large number of laser pulses. And the total ablated mass per area was a function of the energy per area as shown in Fig. 5. When the fluence was lower than 15.92 J/cm², the function within experimental errors was fitted by the straight line $m = K_1 \times (F - F_1)$. *m* and *F* represent the (ablation mass)/(spot size) and the laser fluence, respectively. Furthermore, when the fluence exceeded 15.92 J/cm², the function within experimental errors was also fitted by the straight line $m = K_2 \times (F - F_2)$. And the fitting parameters

K_1, F_1, K_2, and F_2 obtained by the least squares method were 2.906 μg/J, 0.3052 J/cm^2, 0.7308 μg/J, and -46.38 J/cm^2, respectively. K_1 and K_2 can be defined as the mass removal rate. It was reported that the ablation thickness of the material depended directly on the fluence [25]; that is, the higher fluence was expected to generate more ablated material. However, when the laser fluence was greater than 15.92 J/cm^2, the increase of the (ablation mass)/(spot size) slowed down. And the mass removal rate declined to 0.7308 μg/J at the fluence above 15.92 J/cm^2. The decrease of the mass removal rate by pulsed laser ablation would be caused by the plasma shielding effect at the higher laser fluence. In this case, part of the incoming laser energy was absorbed by the plasma plume. As a result, it led to the less laser energy to ablate the target material.
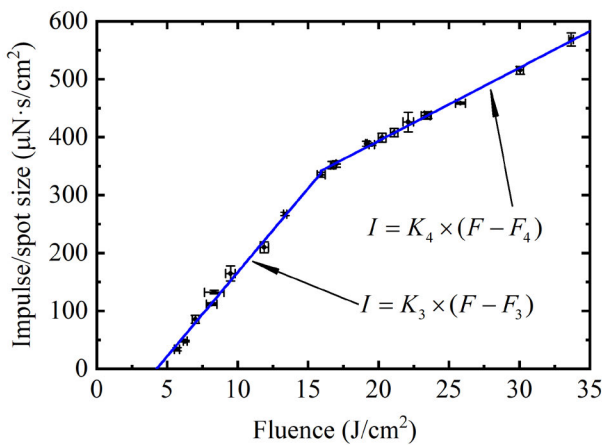

FIGURE 6. Diagram illustrating the variation of the (impulse)/(spot size) irradiated by different laser fluences. The two solid lines (blue) represent fitting with a straight line function respectively. Where *I* and *F* represent the (Impulse)/(spot size) and laser fluence, respectively. $K_3 = 28.98\,\mu$N·s/J, $F_3 = 4.247$J/cm^2, $K_4 = 12.63\,\mu$N·s/J, and $F_4 = -11.15$J/cm^2 were obtained by the least squares method.

Fig. 6 presents the dependence of the (impulse)/(spot size) generated by the laser irradiating the aluminum target on the laser fluence. The laser fluence in the experiment, which was a ratio of the laser pulse energy to the spot size, ranged from the minimum ablation value of 5.69 J/cm^2 to the maximum achievable fluence of 33.67 J/cm^2. Correspondingly, the input laser power density ranged from 6.5×10^8 W/cm^2 to 3.87×10^9 W/cm^2, which resulted in the evaporation of the target material and eventually the formation of a plasma plume. The minimum fluence that led to the impulse generation observed in the experiment was about 5.69 J/cm^2, which agreed reasonably well with the results reported by Torrisi *et al.* [26]. This minimum fluence was related with the laser wavelength, and the IR laser radiation was more efficient for ablating aluminum, resulting in a lower ablation threshold [27]. The results in Fig. 6 showed that the (impulse)/(spot size) increased gradually until the fluence reached 15.92 J/cm^2. The variation of the impulse could be interpreted in terms of the ejected plume. The higher the

laser fluence was, the stronger the intensities of the evaporation and the plasma plume were, and the higher the recoil impulse to the target was. When the fluence was lower than 15.92 J/cm^2, the function within experimental errors could be approximated by the straight line $I = K_3 \times (F - F_3)$. I and F represent the (impulse)/(spot size) and the laser fluence, respectively. However, when the fluence was greater than 15.92 J/cm^2, the increase of (impulse)/(spot size) became slower. And the experimental data within experimental errors were also fitted by the straight line $I = K_4 \times (F - F_4)$. The fitting parameters K_3, F_3, K_4, and F_4 were 28.98 μN·s/J, 4.247 J/cm^2, 12.63 μN·s/J, and -11.15 J/cm^2, respectively.
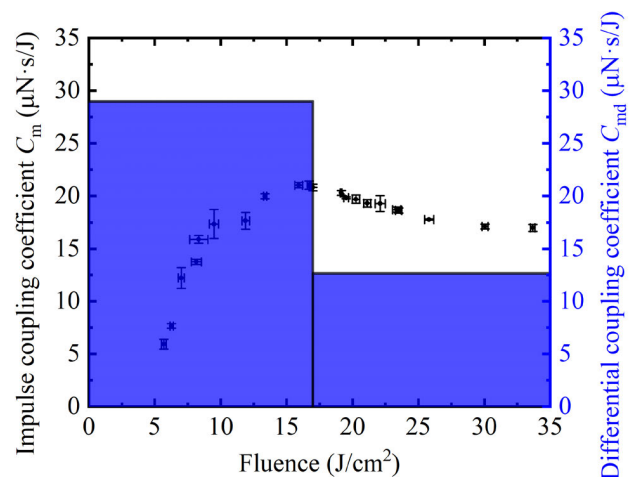

FIGURE 7. The variation of the impulse coupling coefficient C_m and the differential coupling coefficient C_{md} with the laser fluence.

In an attempt to analyze the thrust performance with nanosecond laser ablation, the impulse coupling coefficient C_m, which was the radio of the impulse to the incident laser energy, was employed. Fig. 7 shows the relationship between the impulse coupling coefficient C_m and the laser fluence. The graph reveals that there was a sharp rise of C_m before the maximal coupling coefficient of 21.04 μN·s/J was reached at the fluence of 15.92 J/cm^2. The maximal $C_m = 21.04\mu N \cdot$s/J agreed reasonably well with the experimental data observed by D'Souza when irradiating an aluminum target with nanosecond laser pulses [28]. With the further increase of the laser fluence, C_m began to decline slowly. The trend of C_m shown in Fig. 7 was consistent with the conclusion summarized by Phipps *et al.*[29]. The common cause of the reduction of C_m at higher fluence was described as a consequence of the plasma shielding effect [13]. Based on the results in Fig. 6, K_3 and K_4 also have some sense, which can reflect the laser ablation performance in a different way. We defined the slope coefficient, K_3 and K_4, as the differential coupling coefficient C_{md}. As shown in Fig. 7, the $C_{md} = 28.98\ \mu$N·s/J at the fluence below 15.92 J/cm^2 was slightly greater than the maximum impulse coupling coefficient. However, when the fluence was greater than 15.92 J/cm^2, C_{md} decreased to 12.63 μN·s/J which was close

to the C_m at the fluence of 33.67 J/cm^2. The sharp decline of the C_{md} in these two intervals would be a reasonable account to explain the effect of plasma shielding.

B. COMPARISON OF PLASMA PLUME IMAGES WITH IMPULSE COUPLING COEFFICIENTS

Fig. 8 shows the optical emission spectrum from the plasma plume of neutral atoms (Al I) and ionized ions (Al II, Al III) in the wavelength region of 350-650 nm. The distribution of the charge states was consistent with the results obtained by Shaim *et al.* [30]. The wavelengths of the atomic and ionic emission lines shown in Fig. 8 were identified according to the NIST database. As can be seen, Al$^+$ was the main Al charge state, which corresponded to the results reported by Caridi *et al.*[31]. Therefore, the Al$^+$ whose spectral line appeared at the wavelength of 624.33 nm could be selected as the representative species to analyze the ion plume images.
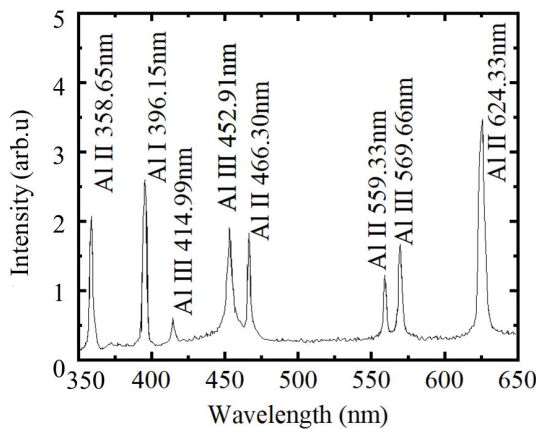

FIGURE 8. The typical spectral emission from the Al plasma plume at the fluence of 15.92 J/cm^2, with an integration time of 1 ms.

Fast photography, which could provide the overall plume self-emission in the spectral window of the ICCD, was used to obtain the 2D maps. The images of the plume morphology, recorded with a gate width of 500 ns after the pulsed laser ablated for different laser fluences, are shown in Fig. 9(a). The plume structures were approximately hemispherical for all the fluences. The emission intensity was more distinguished for the condition of a fluence higher than 15.92 J/cm^2. This could be interpreted with the result of [31] that the charges state increased with the laser fluence and the energetic distributions shifted towards higher energies. Additionally, with the increase of the laser fluence, the highest radiation intensity region in the plasma plume located above the target surface was observed, and it was called the plasma core [17]. The core, which consisted of a large amount of energetic plasma species, was formed via absorbing the incoming laser [32].

In order to record the time-integrated Al$^+$ ions emission plume images, a visible bandpass filter, with a center wavelength of 625 nm and a full width at half maximum (FWHM) of 10 nm, was kept in front of the ICCD during the experiment. The bandpass filter helped to transmit a well-defined wavelength band of optical emission, while rejecting other unwanted radiation. The plume images of Al$^+$ ions obtained with the filter are shown in Fig. 9(b). It can be clearly seen in the emission images that the Al$^+$ emission intensity was not observed in the figure when the fluence was relatively lower. The reason for this was that the plume mostly contained vapor materials corresponding to a lower ionization degree. The emission counts were more distinguished when the fluence exceeded 15.92 J/cm^2. As the fluence grew, the emission intensity was brighter and the emission areas in the figure were larger. Generally, the increase of ionic components and fractional ionizations with the increase of the laser fluence was considered to be a reasonable cause for the phenomenon [26]. Moreover, the energy of the neutral and charged species was high at a higher laser fluence [31], as a result of the inverse bremsstrahlung (IB) for the near-infrared laser wavelength [33].

Typical emission images for the plasma plume corresponding to the C_m at different laser fluences are shown in Fig. 10. The emission intensity was weak at the fluence lower than about 10 J/cm^2, with a smaller generated impulse driven mostly by the target surface vaporization [34]. With the increase of the fluence, the radiation intensity of plasma plume increased gradually and the C_m rose. When C_m reached the maximum at the fluence of around 15.92 J/cm^2, the radiation intensity of the plume became brighter. Furthermore, when the fluence continued to enlarge, C_m decreased as the plasma core appeared and the ion emitting intensity became lighter, which indicated that part of the incident laser energy was absorbed by the plasma plume, other than what was transmitted to the aluminum target surface. The comparison of the C_m and the radiation images illustrated that the optimum C_m occurred in the circumstance of the initial ionization of the plume [34].

C. PLASMA PROPERTIES

Electron temperatures and electron number densities are significant parameters for understanding plasma characteristics generated by laser ablation. In this study, the optical emission spectrum obtained by spectroscopy was used to study the electron temperature and the electron number density. The plasma temperature could be calculated with the Boltzmann plot method using the following equation [35]:

$$T_e = \frac{E_2 - E_1}{k}\left[\ln\left(\frac{I_1\lambda_1 g_2 A_2}{I_2\lambda_2 g_1 A_1}\right)\right]^{-1} \qquad (2)$$

where T_e and k represent the plasma electron temperature and the Boltzmann constant. E_1 and E_2 are the level energy of the two spectral lines, which belonged to the same species. I_1 $\lambda_1 g_1$ and A_1 denote the overall intensity obtained by integrating the profile of the spectral line, the wavelength of the line, the degeneracy, and the transition probability with level E_1, respectively. The subscript 2 indicates that the parameters correspond to the level energy E_2. Fig. 8 gives the typical optical emission spectrum for the laser ablation of aluminum. The ionic lines of Al II appeared at the wavelengths
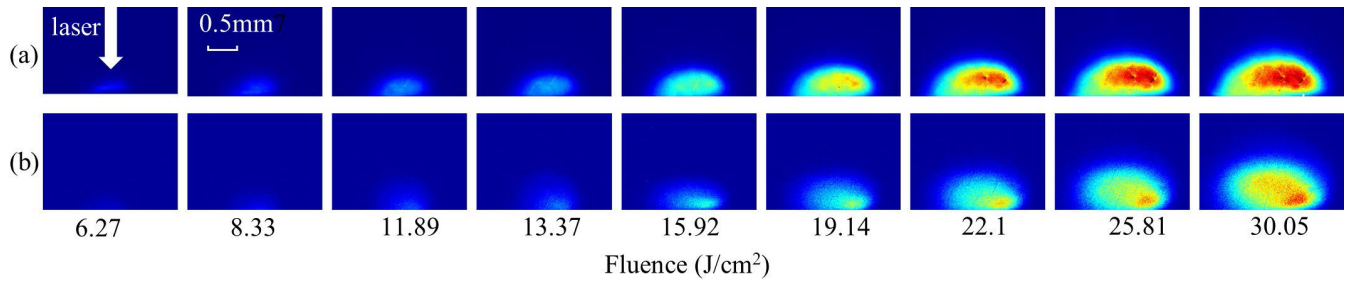
FIGURE 9. ICCD images of (a) the full plasma plume and (b) the Al^+ plumes recorded for different laser fluence values with an exposure time of 500 ns.
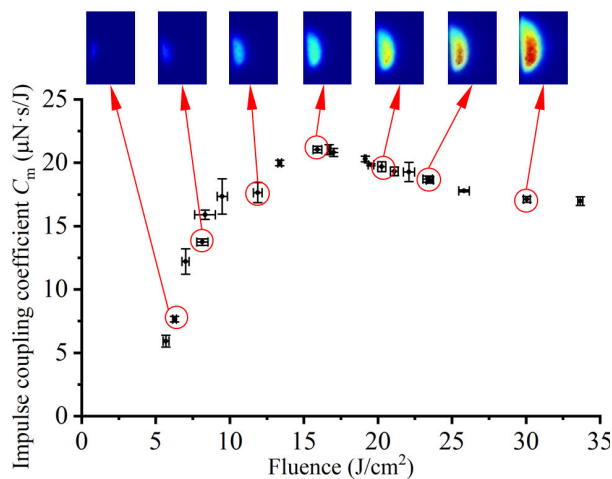

FIGURE 10. Some typical time-integrated images of the plasma plume corresponding to the impulse coupling coefficient at various laser fluences.

FIGURE 11. Plots of the electron temperature kT_e for the Al plasma plume generated by laser ablation and the impulse coupling coefficient C_m at different fluences.

of 624.34 nm, 559.33 nm, 466.30 nm, and 358.66 nm were selected to estimate the electron temperature kT_e. Fig. 11 shows the change of the electron temperature with the laser fluence. A rapid increase occurred in electron temperature until the C_m reached the maximum value, and then the electron temperature increased slowly as the laser fluence increased.

For the optically thin plasma, the electron number density N_e could be calculated by the following equation [19]:

$$\Delta\lambda_{1/2} = 2\omega \left(\frac{N_e}{10^{16}}\right) \qquad (3)$$

where $\Delta\lambda_{1/2}$ is the full width at half maximum (FWHM) of the Stark broadened line. In this study, the spectral line of Al^+ at 624.33 nm that was fitted by the Lorentzian function was used to measure $\Delta\lambda_{1/2}$. ω was the impact factor which could be obtained from [36]. Fig. 12 shows the electron number densities N_e of the plasma plumes ablated by various laser fluences. The values of kT_e and N_e at different fluences were consistent with the results obtained by Shaim *et al.* [30]. As shown in Fig. 12, N_e first increased significantly before the fluence of 15.92 J/cm² corresponding to the maximum C_m. When the laser fluence was greater than
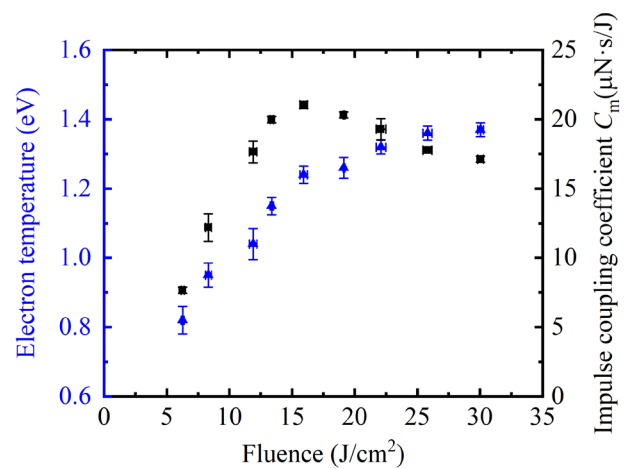
15.92 J/cm², N_e increased slowly with the slight decay of C_m as the fluence increased.

The above calculation of kT_e and N_e was carried out for the LTE hypothesis. To fulfill the LTE conditions, the minimum N_e had to satisfy the following equation [30]:

$$N_e \left(\text{cm}^{-3}\right) \geq 1.6 \times 10^{12} \, [T_e(K)]^{\frac{1}{2}} \, [\Delta E(\text{eV})]^3 \qquad (4)$$

where ΔE is the largest energy level difference. The minimal kT_e at the fluence of 6.27 J/cm² was 0.82 eV, which corresponded to 9515 K. Accordingly, the critical value of N_e was 7.5896×10^{15} cm⁻³. Obviously, the values of N_e shown in Fig. 12 were larger than the critical value; that is, the plasma generated by the laser ablation in the experiment fulfilled the LTE conditions.

By comparing Fig. 11 and Fig. 12, we could find that kT_e and N_e exhibited similar trends with the increase of the laser fluence. At low fluence, kT_e and N_e were both lower with a weaker jet of the plasma plume, resulting in a smaller value of C_m. As the fluence increased, both kT_e and N_e increased rapidly, which led to the enhanced jet of the plasma plume. Therefore, C_m improved until the maximum with the increase of the laser fluence. However, a slower growth occurred in
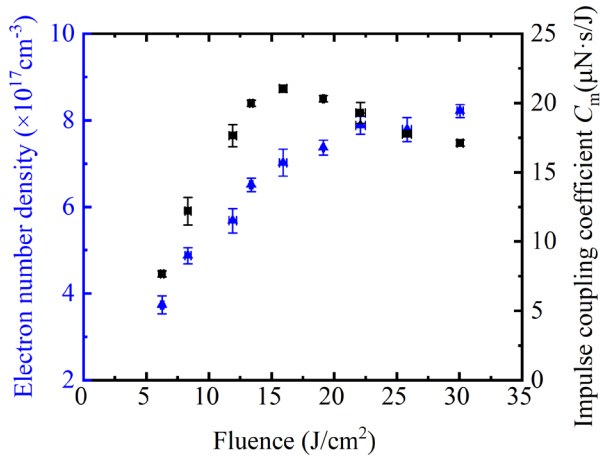
FIGURE 12. Plots of the electron number density N_e for the Al plasma plume generated by laser ablation and the impulse coupling coefficient C_m at different fluences.

both kT_e and N_e due to the plasma shielding effect [37], which also caused the decline of C_m at higher fluences.
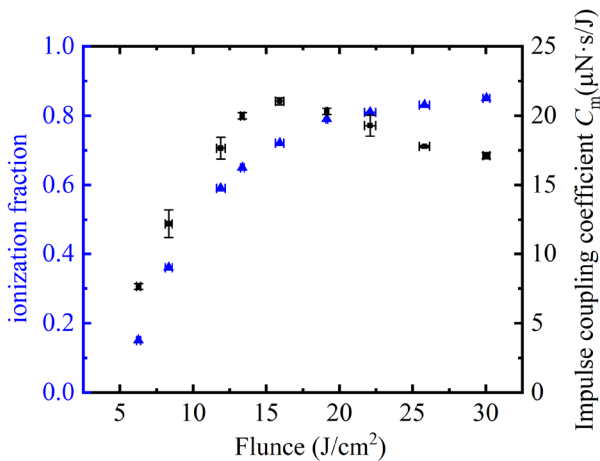

FIGURE 13. Plots of the ionization fraction ζ for the Al plasma plume generated by laser ablation and the impulse coupling coefficient C_m at different fluences.

To analyze the effect of the plasma plumes on the impulse coupling characteristics, the ionization fraction, which could indicate the degree of ionization of the plasma plume, was employed. Based on the model proposed by Sinko and Phipps [38], the ionization fraction was estimated as shown in Fig. 13. The results showed that there was a rise of the ionization fraction with the increase of the laser fluence, but the ionization fraction began to increase gradually when the fluence exceeded 15.92 J/cm². Moreover, the ionization fraction was approximately 0.8 when C_m reached the maximum value, which agreed reasonably well with the result reported by Zhao *et al.* [13]. The comparison of C_m and the ionization fractions illustrated the fact that the decline of C_m corresponded to the increase of the ionization fractions. The higher ionization degree led to the appearance of the plasma

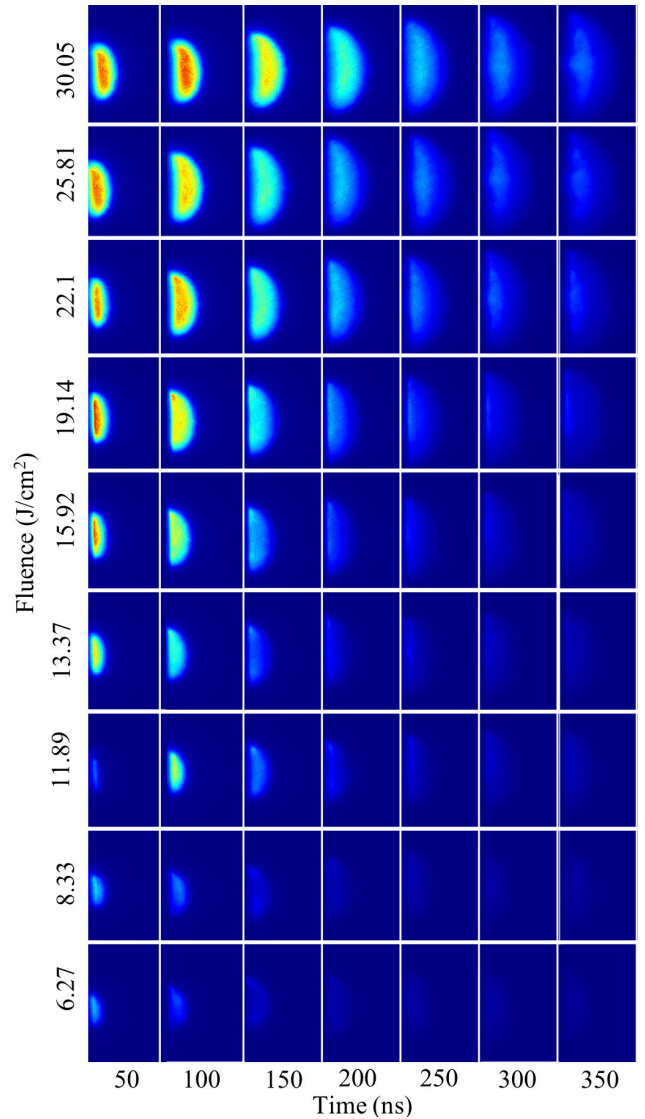core shown in Fig. 9(a) and the so-called enhanced plasma shielding effect.

FIGURE 14. Time-resolved ICCD images of the expanding plume with the gate time of 5 ns for different laser fluences.

D. PLASMA PLUME FRONT ANALYSIS

Time-resolved images of the expanding plasma plume, at varying times within the delay stage of 0-350 ns, are given in Fig. 14. The gate width of the ICCD device was set to 5 ns. In the early phase of the onset of laser-produced plasma, the plume rapidly expanded towards the axial and lateral directions. And the plasma plume generated by laser ablation could also be used to predict the surface roughness in laser polishing process [3]. Besides, it is reported that the luminous boundary of the plasma plume was closely related to the shock wave front, especially in the early period (particularly before 400 ns) [18]. Therefore, the shock wave model was suitable for the front propagation of the laser-induced plasma plume [21]. The Taylor-Sedov equation was employed to

interpret the position change of the plasma plume [24], [39]:

$$R = \varepsilon_0 \left(\frac{E}{\rho_0}\right)^{1/(n+2)} t^{2/(n+2)} \tag{5}$$

$$\varepsilon_0 = \left[\frac{75(\gamma-1)(\gamma+1)^2}{16\pi(3\gamma-1)}\right]^{1/(n+2)} \tag{6}$$

where R, E, ρ_0, t and γ represent the distance from the plasma front to the target surface, the entire energy release that drove the plasma plume, the gas density of the undisturbed ambient, the delay time after ignition, and the specific heat ratio of the gas. For the propagation of the spherical wave, the cylindrical wave, and the plane wave, n was 3, 2, and 1, respectively.

The plasma front position could be inferred from the ICCD images utilizing the $1/e^2$ criterion [17], for which the emission intensity was $1/e^2$ of the maximal intensity in the picture. As deduced from the time-resolved images given in Fig. 14, the position changes for different time delays for different laser fluences were as shown in Fig. 15. The solid line in each picture was fitted with Equation (5) and it could be found that the Taylor-Sedov theory fit the position of the plume front well.
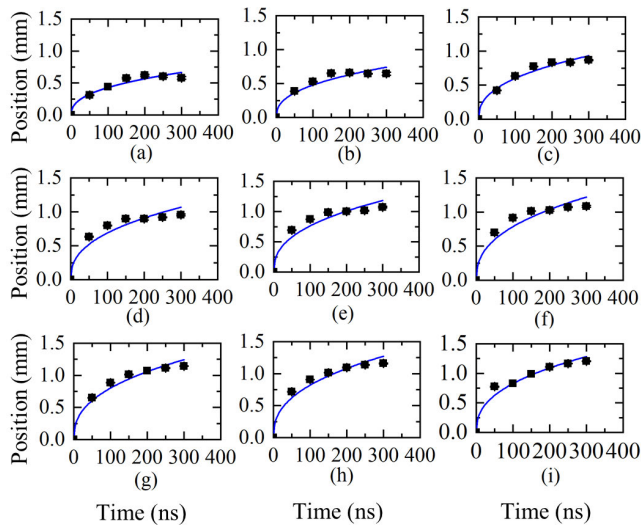

FIGURE 15. R-t plots extracted from the recorded time-resolved images at the fluence of (a) 6.27 J/cm², (b) 8.33 J/cm², (c) 11.89 J/cm², (d) 13.37 J/cm², (e) 15.92 J/cm², (f) 19.14 J/cm², (g) 22.1 J/cm², (h) 25.81 J/cm², (i) 30.05 J/cm². The blue solid curves are the numerical fits to the plasma plume front using Equation (5).

In order to calculate conveniently, Equation (5) could be simplified as follows [18]:

$$R = a_i t^{2/5} \tag{7}$$

where a_i denotes the fitting constant. According to Equations (5) and (7), we obtained the following equation:

$$E_i = \left(\frac{a_i}{\varepsilon_0}\right)^5 \rho_0 \tag{8}$$

where E_i is the energy release that came from the laser-matter interaction process. Because it was difficult to accurately measure the parameters of ε_0 and ρ_0, a dimensionless form deduced from Equation (8) could be written as:

$$e_i = \frac{E_i}{E_1} = \left(\frac{a_i}{a_1}\right)^5 \tag{9}$$

where e_i denotes the relative released energy derived from laser ablation, which could reflect the same variation tendency as E_i with increasing laser fluence. E_1 and a_1 represent the energy release and the corresponding fitting constant at the fluence of ϕ_1, respectively.

Therefore, the energy coupling efficiency η_i [39] at a certain laser fluence could be obtained as follows:

$$\eta_i = \frac{E_i}{E'_i} = \frac{(\frac{a_i}{\varepsilon_0})^5 \rho_0}{E'_i} \tag{10}$$

where E'_i is the initial pulsed laser energy. Equation (10) could be converted to a dimensionless form:

$$\eta'_i = \frac{\eta_i}{\eta_1} = \frac{\frac{E_i}{E'_i}}{\frac{E_1}{E'_1}} = \frac{\left(\frac{a_i}{\varepsilon_0}\right)^5 \rho_0}{E'_i}\frac{E'_1}{\left(\frac{a_1}{\varepsilon_0}\right)^5 \rho_0} = \left(\frac{a_i}{a_1}\right)^5 \frac{E'_1}{E'_i} \tag{11}$$

where η_1 is the energy coupling efficiency at the fluence of ϕ_1 and E'_1 represents the lowest pulsed laser energy in the experiment. Additionally, η'_i denotes the relative energy coupling efficiency, which could reflect the same variation tendency as η_i with increasing laser fluence. The variations of C_m, e_i, and η'_i that depended on laser fluences are shown in Fig. 16.
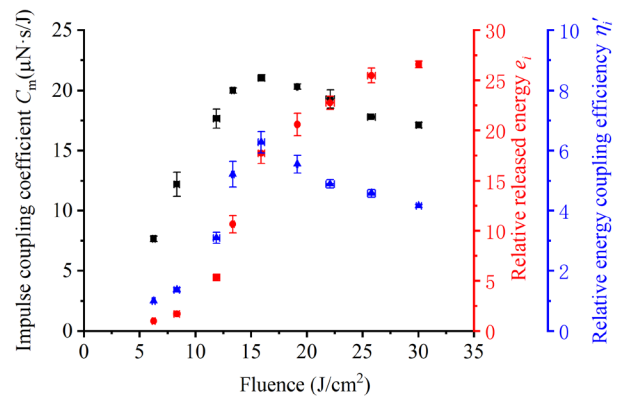

FIGURE 16. The comparisons of the impulse coupling coefficient C_m, the relative released energy e_i, and the relative energy coupling efficiency η'_i at various laser fluences.

What is interesting in this figure is that the trend of η'_i that depended on the laser fluence was similar to that of C_m. There were two possible reasons to explain the phenomenon. First, when the laser fluence was less than 15.92 J/cm², the main component of the plume rapidly changed from the vapor materials to the plasma with the increase of the fluence, leading to a sharp increase of both the relative released energy e_i and the relative energy coupling efficiency η'_i. Second, because the fluence was higher than 15.92 J/cm², the ionization degree of the plume became high with the increased

laser fluence, as shown in Fig.13. As a result, the growing speed of e_i became slow. Therefore, both η_i' and C_m decreased gradually with the high ionization degree of the plume that produced the enhanced plasma shielding.

IV. CONCLUSION

The ablation impulse was measured experimentally with a torsion pendulum. To analyze the thrust performance, the impulse coupling coefficient was calculated. The experimental results showed that the impulse coupling coefficient began to decline once the plasma shielding effect was strong enough.

Images of the plasma plume were simultaneously recorded with the ICCD device. The emission intensity of the Al^+ plume was more distinguished when the fluence exceeded 15.92 J/cm^2. The drop phase of the impulse coupling coefficient C_m corresponded to high radiation images of the plume with a plasma core. The core, which consisted of a large amount of electrons and ions, absorbed incoming laser energy, resulting in the plasma shielding effect. The images of the plasma plume provided a better understanding of the effect of the ablation plume on impulse coupling characteristics.

The plasma temperature kT_e and the electron number density N_e, which were critical parameters for understanding plasma characteristics, were estimated using optical emission spectroscopy. The results showed that kT_e and N_e exhibited similar trends with the increase of the laser fluence. Additionally, both kT_e and N_e showed slower growth when the C_m decreased.

The relative energy coupling efficiency was deduced from the time-resolved emission front, and it could reflect the energy release of the plume. What was interesting was that the trend of the dimensionless efficiency that depended on the laser fluence was similar to that of the impulse coupling coefficient. The obtained results might suggest a useful method for subsequent experiments about the impact of plume dynamics on impulse coupling.

REFERENCES

[1] G. C. Gomes, F. F. Borghi, R. O. Ospina, E. O. López, F. O. Borges, and A. Mello, "Nd:YAG (532 nm) pulsed laser deposition produces crystalline hydroxyapatite thin coatings at room temperature," *Surf. Coatings Technol.*, vol. 329, pp. 174–183, Nov. 2017.

[2] S. Martínez, A. Lamikiz, E. Ukar, A. Calleja, J. A. Arrizubieta, and L. N. L. De Lacalle, "Analysis of the regimes in the scanner-based laser hardening process," *Opt. Lasers Eng.*, vol. 90, pp. 72–80, Mar. 2017.

[3] E. Ukar, A. Lamikiz, S. Martínez, I. Tabernero, and L. N. L. D. Lacalle, "Roughness prediction on laser polished surfaces," *J. Mater. Process. Technol.*, vol. 212, no. 6, pp. 1305–1313, Jun. 2012.

[4] R. Weber, T. Graf, P. Berger, V. Onuseit, M. Wiedenmann, C. Freitag, and A. Feuer, "Heat accumulation during pulsed laser materials processing," *Opt. Express*, vol. 22, no. 9, pp. 11312–11314, May 2014.

[5] R. W. Coons, S. S. Harilal, S. M. Hassan, and A. Hassanein, "The importance of longer wavelength reheating in dual-pulse laser-induced breakdown spectroscopy," *Appl. Phys. B, Lasers Opt.*, vol. 107, no. 3, pp. 873–880, Jun. 2012.

[6] J. E. Sinko, "Laser ablation propulsion tractor beam system," *J. Propuls. Power*, vol. 26, no. 1, pp. 189–191, Jan. 2010.

[7] C. R. Phipps, "L'ADROIT—A spaceborne ultraviolet laser system for space debris clearing," *Acta Astronautica*, vol. 104, no. 1, pp. 243–255, Nov. 2014.

[8] C. R. Phipps, J. R. Luke, T. Lippert, M. Hauer, and A. Wokaun, "Micropropulsion using laser ablation," *Appl. Phys. A, Solids Surf.*, vol. 79, nos. 4–6, pp. 1385–1389, Sep. 2004.

[9] R. Kumar and R. J. Sedwick, "Despinning orbital debris before docking using laser ablation," *J. Spacecraft Rockets*, vol. 52, no. 4, pp. 1129–1134, Jul. 2015.

[10] H. Tsuruta, B. Wang, Y. Katagiri, and A. Sasoh, "Influence of illuminating angle on impulse characteristics with pulsed laser ablation," presented at the Int. Electr. Propuls Conf, Hyogo, Japan, Jul. 2015.

[11] C. Phipps, W. Bohn, T. Lippert, A. Sasoh, W. Schall, and J. Sinko, "Review: Laser-ablation propulsion," *J. Propuls. Power*, vol. 26, no. 4, pp. 609–637, Aug. 2010.

[12] D. Tran, A. Yogo, H. Nishimura, and K. Mori, "Impulse and mass removal rate of aluminum target by nanosecond laser ablation in a wide range of ambient pressure," *J. Appl. Phys.*, vol. 122, no. 23, Dec. 2017, Art. no. 233304.

[13] X.-T. Zhao, F. Tang, B. Han, and X.-W. Ni, "The influence of laser ablation plume at different laser incidence angle on the impulse coupling coefficient with metal target," *J. Appl. Phys.*, vol. 120, no. 21, Dec. 2016, Art. no. 213103.

[14] H. Tsuruta, O. Dondelewski, Y. Katagiri, B. Wang, and A. Sasoh, "Ablation spot area and impulse characteristics of polymers induced by burst irradiation of 1 μm laser pulses," *Acta Astronautica*, vol. 136, pp. 46–54, Jul. 2017.

[15] B. Wang, "Laser ablation impulse generated by irradiating aluminum target with nanosecond laser pulses at normal and oblique incidence," *Appl. Phys. Lett.*, vol. 110, no. 1, Jan. 2017, Art. no. 014101.

[16] K. Suzuki, K. Sawada, R. Takaya, and A. Sasoh, "Ablative impulse characteristics of polyacetal with repetitive CO2 laser pulses," *J. Propuls. Power*, vol. 24, no. 4, pp. 834–841, Jul. 2008.

[17] X. Li, W. Wei, J. Wu, S. Jia, and A. Qiu, "The influence of spot size on the expansion dynamics of nanosecond-laser-produced copper plasmas in atmosphere," *J. Appl. Phys.*, vol. 113, no. 24, Jun. 2013, Art. no. 243304.

[18] S. S. Harilal, G. V. Miloshevsky, P. K. Diwakar, N. L. LaHaye, and A. Hassanein, "Experimental and computational study of complex shock-wave dynamics in laser ablation plumes in argon atmosphere," *Phys. Plasmas*, vol. 19, no. 8, Aug. 2012, Art. no. 083504.

[19] A. E. Hussein, P. K. Diwakar, S. S. Harilal, and A. Hassanein, "The role of laser wavelength on plasma generation and expansion of ablation plumes in air," *J. Appl. Phys.*, vol. 113, no. 14, Apr. 2013, Art. no. 143305.

[20] D. Campos, S. S. Harilal, and A. Hassanein, "The effect of laser wavelength on emission and particle dynamics of sn plasma," *J. Appl. Phys.*, vol. 108, no. 11, Dec. 2010, Art. no. 113305.

[21] P. Sankar, H. D. Shashikala, and R. Philip, "Effect of laser beam size on the dynamics of ultrashort laser-produced aluminum plasma in vacuum," *Phys. Plasmas*, vol. 26, no. 1, Jan. 2019, Art. no. 013302.

[22] X. Jin, Y. Hong, W. Zhou, and H. Chang, "A parameter calibration method for torsion pendulum using in micro thrust and impulse measurement," *J. Propuls. Technol.*, vol. 36, no. 10, pp. 1554–1559, Oct. 2015.

[23] W. Ming, L. Nanlei, and W. Jie, "Experimental study on impulse coupling characteristics of 532 nm/1 064 nm laser ablated Al target," *Infr. Laser Eng.*, vol. 46, no. S1, pp. 1–5, Dec. 2017.

[24] L. Torrisi, M. Cutroneo, and A. Torrisi, "Laser-generated cu plasma in vacuum and in nitrogen gas," *Vacuum*, vol. 178, Aug. 2020, Art. no. 109422.

[25] E. Ukar, A. Lamikiz, L. N. López De Lacalle, S. Martinez, F. Liébana, and Tabernero, "Thermal model with phase change for process parameter determination in laser surface processing," *Phys. Procedia*, vol. 5, pp. 395–403, Jan. 2010.

[26] L. Torrisi, L. Andò, S. Gammino, J. Kràsa, and L. Làska, "Ion and neutral emission from pulsed laser irradiation of metals," *Nucl. Instrum. Methods Phys. Res. Sect. B, Beam Interact. with Mater. At.*, vol. 184, no. 3, pp. 327–336, Nov. 2001.

[27] L. Torrisi, A. Borrielli, and D. Margarone, "Study on the ablation threshold induced by pulsed lasers at different wavelengths," *Nucl. Instrum. Methods Phys. Res. Sect. B, Beam Interact. With Mater. At.*, vol. 255, no. 2, pp. 373–379, Feb. 2007.

[28] B. C. D'Souza, "Development of impulse measurement techniques for the investigation of transient forces due to laser-induced ablation," M.S. thesis, Dept. Aerosp. Mech. Eng., Univ. Southern California, Los Angeles, CA, USA, 2007.

[29] C. Phipps, J. Luke, D. Funk, D. Moore, J. Glownia, and T. Lippert, "Laser impulse coupling at 130 fs," *Appl. Surf. Sci.*, vol. 252, no. 13, pp. 4838–4844, Nov. 2005.

[30] M. H. A. Shaim and H. E. Elsayed-Ali, "Characterization of laser-generated aluminum plasma using ion time-of-flight and optical emission spectroscopy," *J. Appl. Phys.*, vol. 122, no. 20, Nov. 2017, Art. no. 203301.

[31] F. Caridi, L. Torrisi, D. Margarone, A. Picciotto, A. M. Mezzasalma, and S. Gammino, "Energy distributions of particles ejected from laser-generated pulsed plasmas," *Czechoslovak J. Phys.*, vol. 56, no. S2, pp. B449–B456, Oct. 2006.

[32] D. Marla, U. V. Bhandarkar, and S. S. Joshi, "Critical assessment of the issues in the modeling of ablation and plasma expansion processes in the pulsed laser deposition of metals," *J. Appl. Phys.*, vol. 109, no. 2, Jan. 2011, Art. no. 021101.

[33] D. Breitling, H. Schittenhelm, P. Berger, F. Dausinger, and H. Hügel, "Shadowgraphic and interferometric investigations on nd:YAG laser-induced vapor/plasma plumes for different processing wavelengths," *Appl. Phys. A, Mater. Sci. Process.*, vol. 69, no. 7, pp. S505–S508, Dec. 1999.

[34] C. R. Phipps, "Modeling CO_2 laser ablation impulse of polymers in vapor and plasma regimes," *Appl. Phys. Lett.*, vol. 95, no. 13, Sep. 2009, Art. no. 131105.

[35] H. R. Griem and W. L. Barr, "Spectral line broadening by plasmas," *IEEE Trans. Plasma Sci.*, vol. PS-3, no. 4, p. 227, Dec. 1975.

[36] W. L. Wiese, "Experimental stark widths and shifts for spectral lines of neutral and ionized atoms (A critical review of selected data for the period 1989 through 2000)," in *Proc. AIP Conf. Proc.*, 2002, pp. 106–115.

[37] P. Zheng, H. D. Liu, J. M. Wang, B. Yu, R. Yang, B. Zhang, X. M. Wang, "Influences of laser pulse energy on physical characteristics of laser-induced aluminum alloy plasma," *Acta Photonica Sinica*, vol. 43, no. 9, pp. 82–86, 2014.

[38] C. R. Phipps, "Modeling CO2 laser ablation impulse of polymers in vapor and plasma regimes," *Appl. Phys. Lett.*, vol. 95, no. 13, Sep. 2009, Art. no. 131105.

[39] L. Jiao, B. S. Truscott, H. Liu, M. N. R. Ashfold, and H. Ma, "Imaging spectroscopy of polymer ablation plasmas for laser propulsion applications," *J. Appl. Phys.*, vol. 121, no. 1, Jan. 2017, Art. no. 013303.

WEIJING ZHOU received the B.S. and M.S. degrees in aircraft design engineering from the Academy of Equipment Command and Technology, Beijing, China, in 2007, and the Ph.D. degree in aircraft launch theory and technology from the Academy of Equipment, Beijing, in 2010.

Since 2011, she has been a Research Assistant with the State Key Lab of Laser Propulsion & Application, Space Engineering University. She has authored three books, more than 30 articles, and more than 15 inventions. Her research interests include micro-thrust measurement, laser ablation micro-thruster, and laser ablation propulsion.

HAO CHANG received the B.S. and M.S. degrees in aircraft power engineering from Aviation University, Changchun, Jilin, China, in 2008, and the Ph.D. degree in aircraft launch theory and technology from the Academy of Equipment, Beijing, in 2014.

Since 2011, he has been a Research Assistant with the State Key Lab of Laser Propulsion & Application, Space Engineering University. From 2017 to 2019, he was a Postdoctoral Research with the China Academy of Space Technology, Beijing. He has authored 1 book, more than 20 articles, and more than 10 inventions. His research interests include laser ablation propulsion, laser orbital debris removal, and optical emission spectrum measurement.

CHENGHAO YU received the B.S. degree from the Shandong University of Technology, China, in 2018. He is currently pursuing the master's degree in aerospace science and technology with Space Engineering University, China.

His current research interest includes laser ablation propulsion.

YIFU CHEN received the bachelor's degree in automation specialty from the Wuchang University of Technology, China. He is currently pursuing the master's degree in aerospace science and technology with Space Engineering University, China.

His current research interest includes laser interaction with matter.

• • •